

Distributed Measurement of Deformation Magnitude and Location with a Pair of Soft Sensors

Mohammed Al-Rubaiai,* Ryohei Tsuruta, Umesh Gandhi, and Xiaobo Tan

Skin-like sensitivity, or the capability to recognize tactile information, is essential for future robots in elder care, search and rescue, entertainment and other applications involving unstructured environments. In this paper, we propose the design of a flexible one-dimensional pressure-sensing system that can localize deformation along a long strip and measure its magnitude with an integrated pair of sensors. The sensor system is fabricated with piezoresistive conductive foils and copper sheets encapsulated by adhesive tape with a total thickness of 0.7 mm. For the purpose of demonstration, the sensor is used to monitor the location and magnitude of kink deformation of an inflatable tube. Finite-element modeling and simulation are conducted to investigate the behavior of the soft sensor system when subjected to kink deformation. The model-predicted sensor output achieves good agreement with the experimental data for different deformation magnitudes. Finally, extensive experiments on a sensor prototype with dimensions of 35×500 mm mounted on an inflatable tube are conducted to demonstrate the capability of the proposed scheme in simultaneous measurement of deformation location and magnitude. It is shown that the specific design approach minimizes the coupling of location and magnitude measurements, resulting in minimal complexity for data processing.

1. Introduction

Recent advancements in robotics have significantly expanded applications in specialized areas, such as healthcare and human–machine interaction (HMI). Examples include elder-assistive robots,^[1,2] healthcare robots through social communication,^[3,4] and interactive educational robots.^[5,6] Safe physical interaction with human users is one of the most important requirements when designing such robots.^[7] Due to their rigid nature, traditional robots typically cannot guarantee safe interaction with humans. While different types of sensors could be used to avoid collisions

with humans,^[8,9] these methods cannot prevent collisions that occur due to control or system errors.

Soft robots offer promising alternatives to overcome the challenges in interacting physically with humans and environments. Highly deformable elastomers are widely used for developing stretchable sensors^[10–15] and compliant actuators that are used in soft robots.^[16–18] Combining soft components with robots could increase their safety levels.^[19] It is even possible to make the entire robot soft, as shown with soft manipulators^[20–22] and wearable robots.^[23–25] Another approach is to cover the entire robot body using inflatable structures,^[26–28] which will provide a certain level of structural safety. However, most of the reported inflatable robots lack the capability to directly sense external contacts through their body structures; such an ability would significantly increase robot responsiveness and autonomy. Pressure-mapping soft sensors have also been explored in HMI robots. Typically, arrays

of pressure transducers are built into the robotic system to provide a large number of discrete pressures measurements at selected locations.^[29–31] However, such a system is both mechanically complex and computationally intensive.

Optoelectronic sensing is another approach to distributed pressure sensing, where deformation is measured through changes in the light that is emitted and received through a light guide. In particular, fiber optic intensity modulation (FOIM)^[32] is a common method that refers to a class of sensing techniques, where light escapes from a light guide in response to some stimulus such as bending of the optical fiber. However, this technique is limited to the assumption that the sensor curvature is uniform as one can only measure the total light loss within the entire sensor. Shape detection is also explored with fiber Bragg gratings (FBGs),^[33] which reflect light with a peak wavelength that shifts in proportion to variations in strain and temperature. While FBG has demonstrated the capability in 3D shape reconstruction, the requirement to maintain the precision spacing of multiple, independent optical fibers throughout a soft structure and the weight of the required equipment presents several manufacturing challenges.

In this article, we propose a novel lightweight, inexpensive, and easy-to-fabricate flexible 1D sensor system that can simultaneously measure the magnitude and the location of deformation along a long strip. The system consists of vertical stacking

M. Al-Rubaiai, X. Tan
Department of Electrical and Computer Engineering
Michigan State University
East Lansing, MI 48824, USA
E-mail: alrubaia@msu.edu

R. Tsuruta, U. Gandhi
Toyota Motor North America
Ann Arbor, MI 48105, USA

 The ORCID identification number(s) for the author(s) of this article can be found under <https://doi.org/10.1002/adem.202101146>.

DOI: 10.1002/adem.202101146

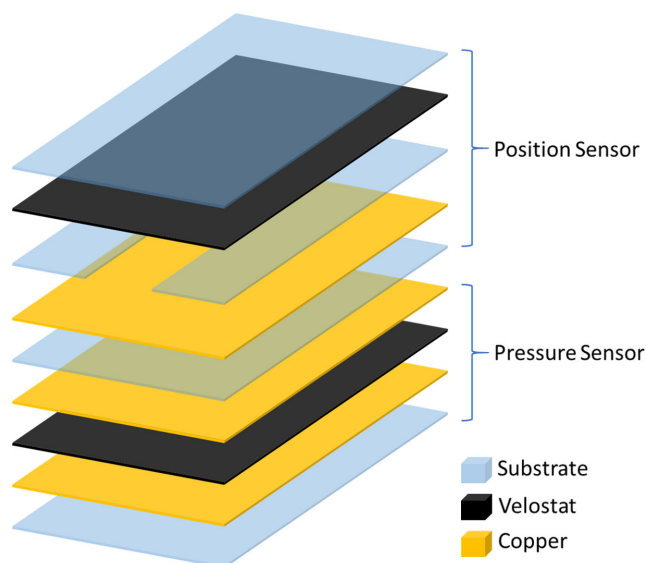


Figure 1. Illustration of the structure of the proposed flexible sensing system, which involves Velostat, copper tapes, and flexible insulating substrate (adhesive tape).

of two sensors, one measuring the location of the deformation and the other measuring its magnitude. Both sensors utilize layers of soft piezoresistive films (Velostat) and copper sheets and their design ensures minimal cross coupling of the two measured quantities. To put the discussion in context, we consider a configuration where the integrated sensor pair is mounted on an inflatable tube, which is subjected to kink deformation, the location and magnitude of which can be independently controlled. Finite-element modeling is conducted to capture the deformation under an applied kink, which is subsequently used to predict the measured sensor output based on the characterized strain–resistivity relationship. The validity of the model is verified with data obtained under kinks of different magnitudes. Finally, we show experimental results obtained from a 500 mm-long sensor, which support the sensor pair’s

capability to simultaneously capture the location and magnitude of the kink applied on the inflatable tube. While this work has demonstrated the applicability of the sensor to inflatable structures, with potential applications in extraterrestrial structure habitats,^[34] inflatable wings,^[35,36] seating comfort,^[37] and inflatable antennas,^[38] the proposed sensor system can be readily tailored to custom dimensions integrated with other substrates such as textiles and elastomers for wearable and soft robot applications.

The remainder of the article is organized as follows. The sensor design and the fabrication process of the soft sensing system are first presented in Section 2. Finite-element modeling and simulation of the deformation and sensor output under a kink stimulus are discussed in Section 3, followed by experimental validation including simultaneous measurement of deformation location and magnitude over the long strip (500 mm) in Section 4. Finally, concluding remarks, including a discussion on future work, are provided in Section 5.

2. Sensor System Design and Fabrication

Figure 1 illustrates the different layers of the proposed soft sensor system. The sensor system consists of a position sensor and a pressure sensor, both of which are fabricated from a commercially available, conductive polymer sheet-like material called Velostat (DESCO Industries) and a carbon-impregnated polymer with piezoresistive properties. Its electrical resistance decreases when pressure is applied. The Velostat piezoresistive behavior is due to a change in the distance between conductive carbon particles that occurs when the material is under stress, as shown in **Figure 2**. With an applied pressure, these particles get closer together, and if this material is sandwiched between two conductors, the resultant structure can act as a pressure or force sensor.^[39]

The pressure magnitude sensor involves one layer of a piezoresistive foil sandwiched between two layers of conductive copper sheets. These layers of copper sheets have an extension for allowing the connection with the external measurement circuit. The layers of piezoresistive material are always larger than the layers of the copper sheets. This is necessary to avoid a

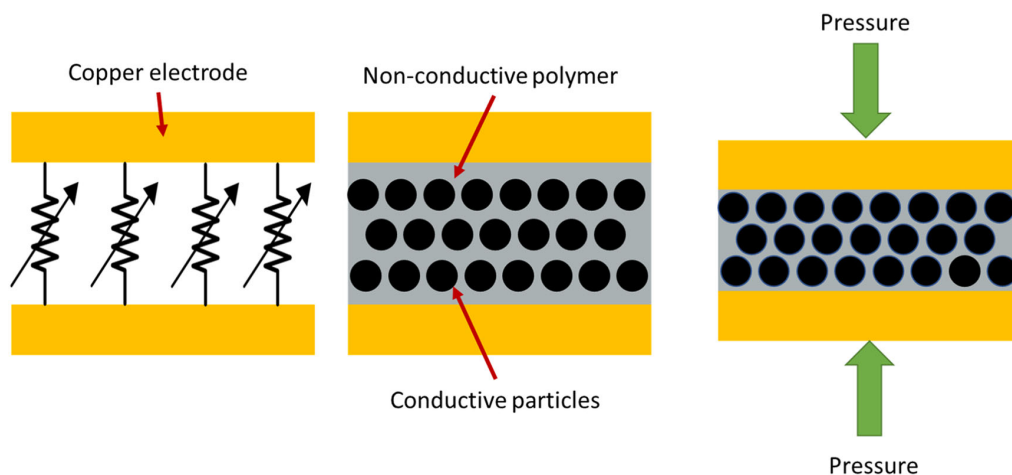


Figure 2. Schematic view of the piezoresistive pressure sensor.

short circuit between the conductors. Finally, the resultant structure is wrapped with nonconductive adhesive tape (NOPI, tesa tape inc.).

As the conductivity of copper ($5.96 \times 10^7 \text{ S m}^{-1}$)^[40] is much higher than that of the piezoresistive layer (0.2 S m^{-1})^[41] the sensor resistance can be viewed as the parallel connection of piezoresistive elements. As such, when an external loading is applied, it reduces the resistance of the corresponding element, the amount of which depends only on the magnitude of loading. Due to the nature of parallel connection of the piezoresistive elements, the resulting sensor output will depend only on the loading magnitude, with negligible dependence on where the loading is applied.

The position sensor uses the concept of a potentiometer and acts as a variable resistor according to the position at which deformation or loading takes place. The sensor is composed of a fully conductive material (copper) layer, an insulated spacing material, and a flexible piezoresistive film, as shown in **Figure 3**. Once a contact results from the loading, the measured resistance is only dependent on the distance of the contact point C to the base point B and thus expected to have a linear relationship with the loading point, with minimal influence from the magnitude of loading (as long as a contact is established). The position-dependent resistance can be readily measured with a voltage-divider circuit.

3. Finite-Element Modeling and Simulation

In this section, we use material properties to create a finite-element method (FEM) model of the soft sensor system. The static structural module in Ansys software is used in this work.

3.1. Simulation of the Pressure Sensor

First, we study the soft pressure sensor (illustrated in **Figure 2**) and examine its strain response when subjected to deformation, which will be further validated with experimental measurement. **Figure 4** shows the FEM simulation setup, where an inflatable tube is fixed from both ends, and the soft pressure sensor is bonded on top of it. Both the sensor and the tube are subjected to a deformation caused

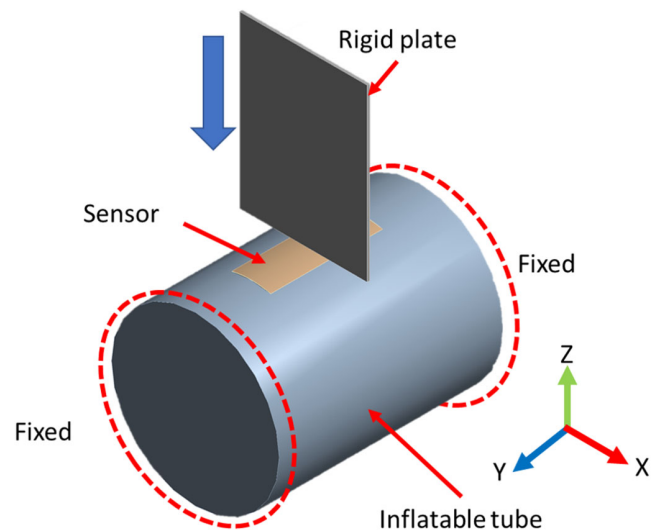


Figure 4. FEM simulation setup for the soft pressure sensor.

by a rigid plate that moves in the negative y-direction. The inflatable tube internal pressure is 3 psi and the dimensions and Young's moduli of all parts in the FEM simulation are listed in **Table 1**

Figure 5 shows the deformation profile in the isometric view when the rigid plate pushes in by 10 mm. In the simulation, the Velostat layer is studied as a grid of 7×20 elements with dimensions $5 \text{ mm} \times 5 \text{ mm} \times 0.1 \text{ mm}$ for each element. The elastic strain profile on the Velostat layer of the sensor under 10 mm deformation (at the point touching the rigid plate) is shown in **Figure 6**, which indicates that maximum strain values are in the proximity of the area of contact with the plate. The strain of the sensor will change when deformation increases or decreases. For example, **Figure 7** shows the simulated axial strain (average of 140 elements) of the Velostat layer in the vertical direction for different deformation values, represented by how much (in mm) the rigid plate is pushed into the tube wall. From the figure, one can see that the strain shows a monotonic (and nearly linear) relationship with the magnitude of the applied deformation.

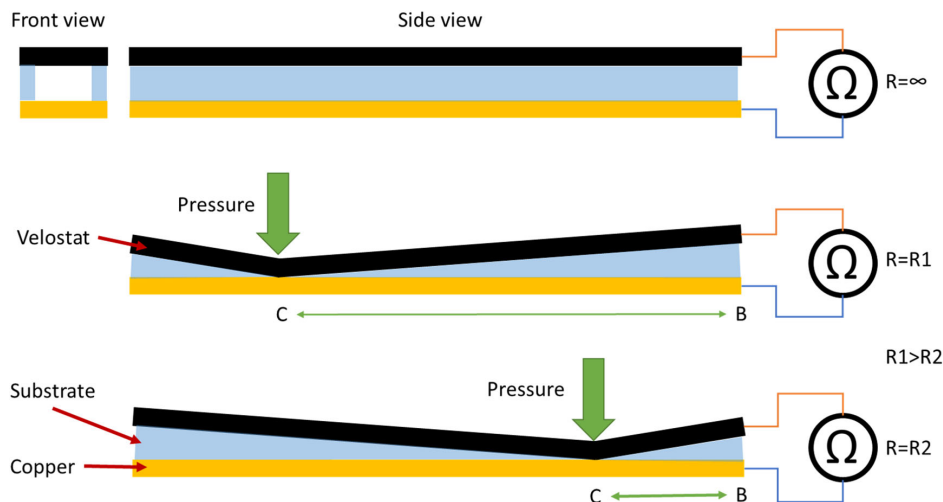


Figure 3. Schematic view of the piezoresistive position sensor.

Table 1. The dimensions and young's moduli of the FEM simulation study.

Part	Material	Length [mm]	Width [mm]	Thickness [mm]	Young's modulus [MPa]
Piezoresistive layer	Velostat	100	35	0.1	180 ^[44]
Spacer	Adhesive tape	100	35	0.1	270 ^[45]
Conductive layer	Copper	100	35	0.07	117 000 ^[40]
Tube	Nylon	500	150	0.4	3000 ^[46]
Kink plate	Aluminum	100	150	2	70 000 ^[40]

3.2. Simulation of the Position Sensor

In the second simulation, we study the soft position sensor (illustrated in Figure 3) and examine the contact area between the Velostat layer and the copper layer when subjected to deformation. This simulation uses the same setup as in Figure 4 but with focus on the soft position sensor. In particular, we are interested in examining how the kink (or pressure) magnitude might interfere with the contact position measurement. The Velostat and the conductive layers have the same dimensions (34 mm × 100 mm), which sandwich two spacers each with dimensions of 15 mm × 100 mm; refer to Figure 3 for illustration. In the simulation, the Velostat layer is studied as a grid of 4 × 100 elements with dimensions 1 mm × 1 mm × 0.1 mm for each element. The area of contact between the Velostat layer and the copper layer under a given plate-induced kink deformation is simulated. **Figure 8** shows the results when the imposed kink deformation is 1, 5, and 10 mm, respectively. From the figure, one can see that the applied deformation magnitude does have an impact on the size of the contact area, which subsequently can influence the measured resistance (the distance between the base point B and the closest contact point C in Figure 3). However, simulation also shows that such impact is

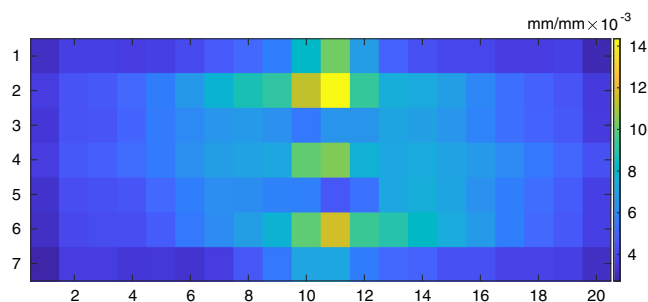


Figure 6. Strain distribution on the Velostat sensing layer under a 10 mm kink deformation caused by the rigid plate.

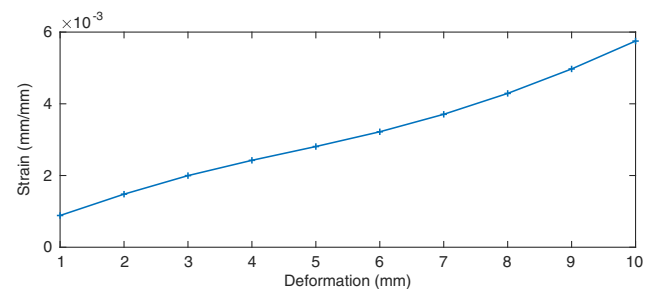


Figure 7. FEM simulation of the average strain distribution on the Velostat sensing layer as the kink deformation increases.

minor, for example, for a kink deformation of 10 mm, the position measurement error is at the order of 0.5 mm, which is consistent with experimental observations shown in Section 4.

4. Experimental Section

To identify the sensitivity of the Velostat piezoresistive material, experiments were implemented to measure the change of resistance in response to the deformation applied. An inflatable tube made with 420D Nylon Fabric from DIY Packraft, USA, was used

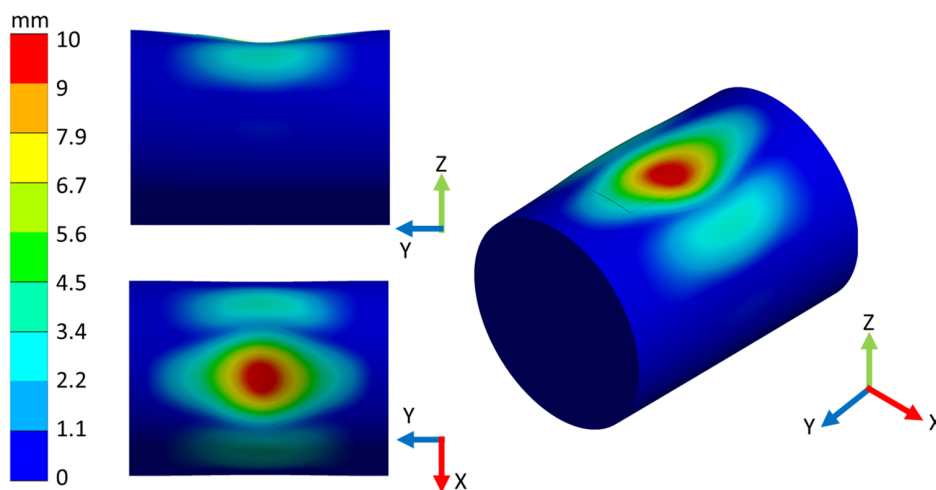


Figure 5. Isometric view of the deformation profile for the soft pressure sensor under a 10 mm kink imposed by the rigid plate.

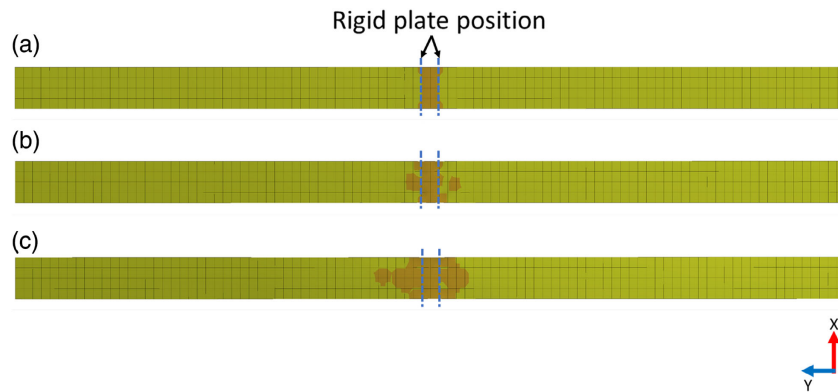


Figure 8. FEM simulation of the contact area distribution (in orange, shaded) on the Velostat sensing layer when the plate-induced kink deformation is a) 1 mm, b) 5 mm, and c) 10 mm.

to test the performance of the flexible sensor system. The inflatable tube had a total length of 100 cm and a cross-sectional radius of 7.5 cm. To introduce deformation to the inflatable tube, an experimental setup shown in **Figure 9** was used. Two linear screw-driven guides, which could move in the vertical and horizontal directions, respectively, were mounted within a rigid cuboid aluminum frame, with both linear screw guides controlled by stepper motors. A rigid plate (150 mm width and 2 mm thickness) was fixed on the vertical linear screw-driven guide to exert kink deformation on the tube and the sensor, and the sensor resistances were measured with two voltage divider circuits. The control of the movement of the rigid plate during the experiments and the data acquisition were implemented with a microcontroller (model number A000073, Arduino).

4.1. Experiments on Magnitude Sensor

First, we mounted a soft pressure sensor patch along with dimensions of 35 mm × 100 mm on the inflatable tube shown in **Figure 10** to validate the FEM results from the previous section. A formulation developed by Zhang et al.^[42] was further utilized to compare the experimental result with the FEM simulation. The formulation was developed for modeling the dependence of the electrical resistivity of semiconductive polymer composites on an applied load.

$$\frac{R}{R_0} = (1 - \varepsilon)e^{-\gamma D\varepsilon[(\pi/(6\phi))^{1/3} - 1]} \quad (1)$$

$$\gamma = \frac{4\pi}{h} \sqrt{2m\phi} \quad (2)$$

where R is the resistance under an imposed strain, R_0 is the initial resistance, ε is the strain, D is the filler particle diameter, ϕ is the volume fraction of filler particles, m is electron mass, ϕ is the height of the potential barrier between two adjacent filler particles, and h is Planck's constant. The parameters used in this work are listed in **Table 2**.

Equation (1) enables one to map the elastic strain from the FEM simulation to the experimental resistance. The calculated resistance profile of the Velostat layer under a kink deformation of 10 mm deformation is shown in **Figure 11**, which indicates that the minimum resistance value is around the center of the contact area. To calculate the equivalent total resistance of the Velostat layer, the segments were considered to be in parallel connection with each other. **Figure 12** shows the average of the five measured resistance values as the deformation is increased and then decreased, along with its comparison with the predictions by the FEM model. It can be seen that, while the FEM simulation did not capture the modest hysteresis observed in experiments, it was able to predict the resistance

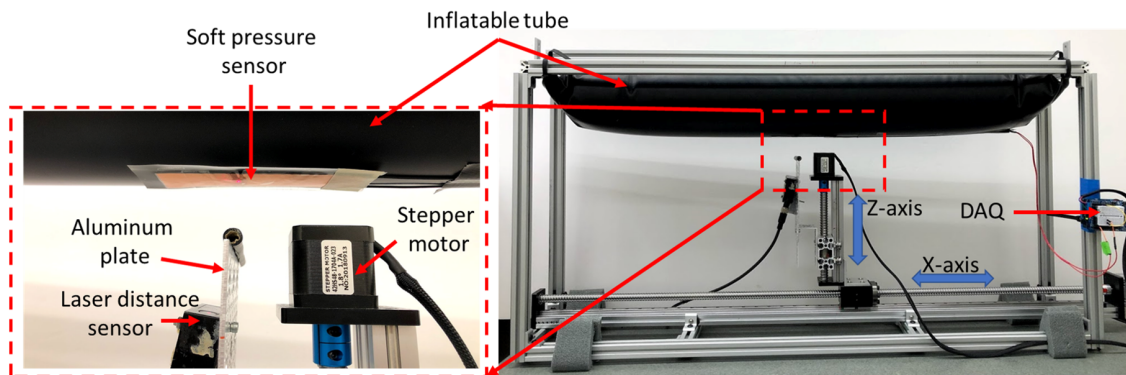


Figure 9. Experimental setup for exerting the deformation on inflatable tube with controlled position and magnitude.

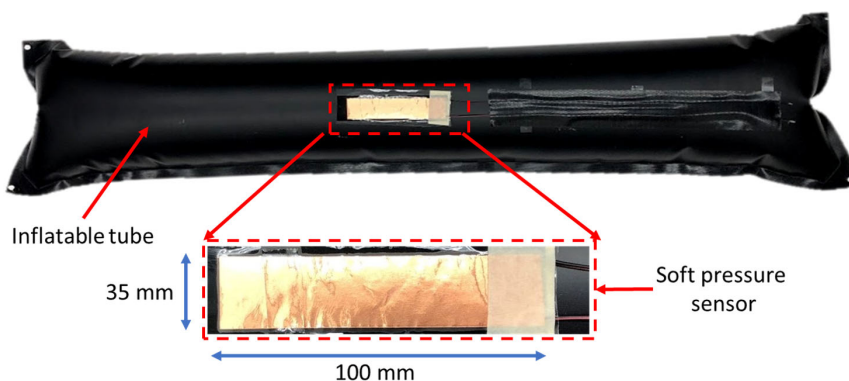


Figure 10. Experimental tube mounted with a 100 mm-long soft pressure sensor patch.

Table 2. Parameters for the model in Equation (1) and (2).

Volume fraction of carbon particle	ϕ	0.2873 ^[42]
Diameter of carbon particle	D	$500 \times 10^{-9} \text{ m}$ ^[42]
Potential height of carbon black and polyethylene	φ	$8.01 \times 10^{-21} \text{ Joule}$ ^[42]
Planck's constant	h	$6.6 \times 10^{-34} \text{ m}^2 \text{ kg s}^{-1}$ ^[47]
Electron mass	m	$9.1 \times 10^{-31} \text{ kg}$ ^[48]

output in general, all the way up to the maximum applied kink deformation of 10 mm.

To characterize the cyclic stability, the soft pressure sensor was further tested by measuring the resistance under repeated cycles of deformation from 0 to 10 mm with steps of 2 mm and the kink deformation speed for the experiment was 2 mm s^{-1} , as shown in Figure 13. The tested sensor exhibited some transient behavior, but the responses were largely stabilized after the first 2000 s (200 cycles). The transient was believed to be linked to the inherent mechanoelectrical dynamics of the material. We also noted that the duration of the transient could vary with the magnitude of the cyclic stimulus, as shown in the study by Dzedzickis et al.^[43]

4.2. Experiments on Full Sensor System

Additional experiments were conducted to test the proposed sensing system composed of both sensor units, as shown in

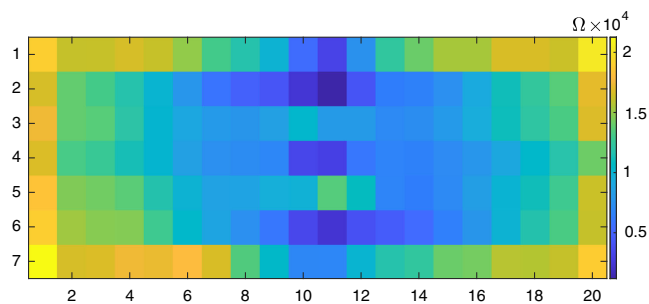


Figure 11. Calculated resistance distribution for the Velostat sensing layer at 10 mm deformation.

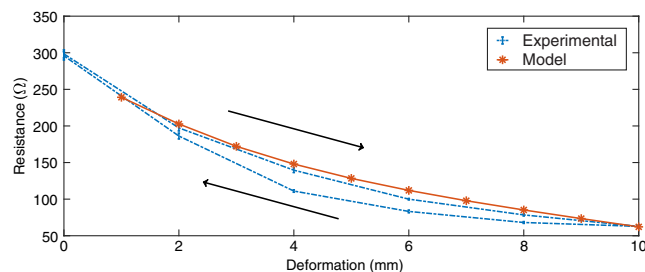


Figure 12. Measured and FEM prediction of the electrical resistance variation with respect to the deformation for the Velostat pressure sensor. The measured resistance shown is the average of five measurements; also shown is the standard deviation of those measurements at each kink deformation.

Figure 1. The sensing system was bonded to the inflatable tube, as shown in Figure 14. The final dimensions of the fabricated sensor system were 35 mm wide, 500 mm long, with a total thickness of 0.7 mm. During the experiment, rigid plate-induced kink deformations of 5, 10, and 15 mm were applied on the tube every 10 mm along the tube, throughout the full sensor length of 500 mm. The results from the position sensors (Figure 15) showed an almost linear relationship between the sensor output and the location of the deformation applied. In particular, it can be seen that the position sensor output was largely consistent when different magnitudes of deformation were applied at the same location, which showed decoupling of the position sensor measurement from applied loading. In particular, while at each location, the measured sensor output was slightly lower with a larger deformation, which was consistent with the simulation, and the differences caused by the deformation magnitude were negligible, also consistent with the simulation finding.

Figure 16 shows the output of the deformation magnitude sensor during the same set of experiments. It can be seen that, under the same magnitude of kink deformation, the sensor output was largely consistent when the deformation was applied at different locations. The standard deviations (for five experiments) in this setup were also small. Combining the outputs from both sensors thus will provide simultaneous measurement of the position and the magnitude of the kink deformation along the inflatable structure.

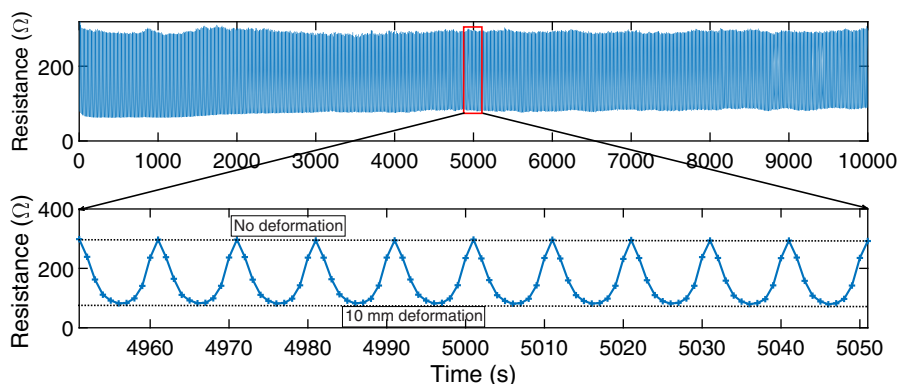


Figure 13. Change in resistance for the Velostat conductive films during cycles of applying and releasing deformation.

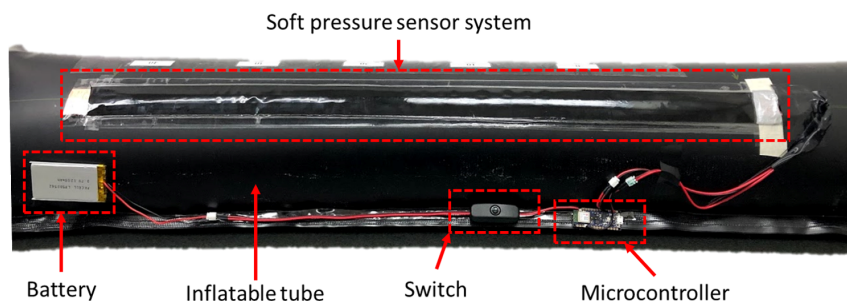


Figure 14. Experimental tube mounted with a 500 mm-long sensor system.

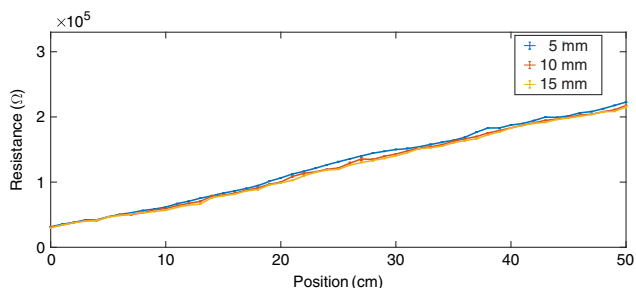


Figure 15. The position sensor output when the deformation is applied along the tube, where each curve represents the results obtained under a given amount of kink deformation.

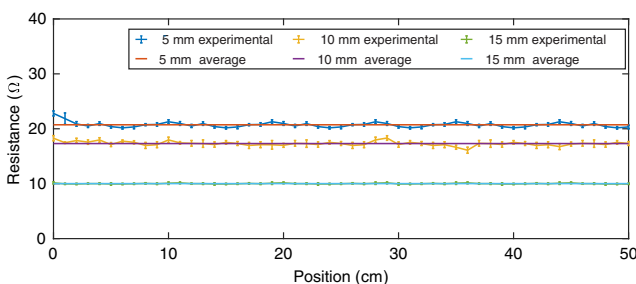


Figure 16. The magnitude sensor output when the kink deformation is applied along the inflatable tube, where the experimental curve represents the results obtained under a given amount of kink deformation and the average curve represents the average of all the data collected at the corresponding deformation.

5. Conclusion and Future Work

In summary, we developed and investigated a real-time soft pressure sensor system that is capable of measuring both the magnitude and location of deformation and evaluated it on an inflatable tube structure. A semiconductive polymer composite, Velostat, was selected to demonstrate the proposed sensor system by means of FEM modeling and experiments. This sensor system provides the advantages of low cost, simplicity in fabrication, robust mechanical properties, and versatility in applications. The mechanical properties of the sensor materials were used in the FEM simulation of the soft sensor system. The simulation results on the elastic strain behavior of the sensor showed a good match with experimental measurements. A sensor system prototype with a length of 50 cm was constructed and evaluated experimentally. Only four electrical leads were needed for the sensing system to simultaneously measure the magnitude and location of deformation along the entire length of the sensing area.

For future work, we will explore different sensor geometries for detecting other deformations (wrinkles and bending angle). The optimal design of the sensor in terms of geometry and material will be further studied with FEM and experiments. While this work has focused only on sensing along a strip, we will investigate the extension to sensing within a 2D area.

Acknowledgements

This work was supported in part by Toyota Motor North America and by an MSU Strategic Partnership Grant (16-SPG-Full-3236).

Conflict of Interest

The authors declare no conflict of interest.

Data Availability Statement

The data that support the findings of this study are available from the corresponding author upon reasonable request.

Keywords

distributed contact monitoring, pressure mapping, soft robotics, soft sensors

Received: August 30, 2021
Revised: November 27, 2021
Published online: January 17, 2022

- [1] Z. Mohamed, G. Capi, *Procedia Eng.* **2012**, *41*, 345.
- [2] M. Vincze, W. Zagler, L. Lammer, A. Weiss, A. Huber, D. Fischinger, T. Koertner, A. Schmid, C. Gisinger, in *41st Int. Symp. on Robotics, VDE, Munich, Germany*, **2014**, pp. 1–7.
- [3] C. Jayawardena, I.-H. Kuo, E. Broadbent, B. A. MacDonald, *IEEE Syst. J.* **2014**, *10*, 1056.
- [4] D. Feil-Seifer, M. J. Matarić, *IEEE Rob. Autom. Mag.* **2011**, *18*, 24.
- [5] D. Felipe Paez Granados, B. A. Yamamoto, H. Kamide, J. Kinugawa, K. Kosuge, *IEEE Rob. Autom. Lett.* **2017**, *2*, 1452.
- [6] M. Fridin, *Comput. Educ.* **2014**, *70*, 53.
- [7] S. Chen, Y. Pang, Y. Cao, X. Tan, C. Cao, *Adv. Mater. Technol.* **2021**, *6*, 2100084.
- [8] D. Kulić, E. Croft, *Auton. Rob.* **2007**, *22*, 149.
- [9] R. Schiavi, A. Bicchi, F. Flacco, in *IEEE Int. Conf. on Robotics and Automation*, IEEE, Piscataway, NJ **2009**, pp. 259–264.
- [10] T. Kim, Y.-L. Park, *IEEE Rob. Autom. Lett.* **2018**, *3*, 881.
- [11] Y.-L. Park, *IEEE Sens. J.* **2012**, *12*, 2711.
- [12] S. Yao, Y. Zhu, *Nanoscale* **2014**, *6*, 2345.
- [13] M. Al-Rubaiai, R. Tsuruta, U. Gandhi, C. Wang, X. Tan, *Smart Mater. Struct.* **2019**, *28*, 134.
- [14] D. Coleman, M. Al-Rubaiai, X. Tan, in *Behavior and Mechanics of Multifunctional Materials XIII*, (Ed: H. E. Naguib), vol. 10968, International Society for Optics and Photonics, SPIE, Bellingham **2019**, pp. 148–156.
- [15] M. Aidi Sharif, H. Lei, M. K. Al-Rubaiai, X. Tan, *Smart Mater. Struct.* **2018**, *27*, 075039.
- [16] J. Wirekoh, Y.-L. Park, *Smart Mater. Struct.* **2017**, *26*, 230.
- [17] L. Paez, G. Agarwal, J. Paik, *Soft Rob.* **2016**, *3*, 109.
- [18] M. Al-Rubaiai, T. Pinto, C. Qian, X. Tan, *Soft Rob.* **2019**, *6*, 318.
- [19] D. Shin, I. Sardellitti, Y.-L. Park, O. Khatib, M. Cutkosky, *Int. J. Rob. Res.* **2010**, *29*, 571.
- [20] J. M. Álvarez Palacio, A. Riwan, N. Mechbal, E. Monteiro, S. Voisembert, in *2017 IEEE Int. Conf. on Advanced Intelligent Mechatronics (AIM)*, IEEE, Piscataway, NJ **2017**, pp. 88–93.
- [21] T. Ranzani, G. Gerboni, *Bioinspiration Biomimetics* **2015**, *10*, 211.
- [22] J. D. Greer, T. K. Morimoto, in *2017 IEEE Int. Conf. on Robotics and Automation (ICRA)*, IEEE, Piscataway, NJ **2017**, pp. 5503–5510.
- [23] Y.-L. Park, B.-R. Chen, N. O. Pérez-Arancibia, D. Young, L. Stirling, R. J. Wood, E. C. Goldfield, R. Nagpal, *Bioinspiration Biomimetics* **2014**, *9*, 160.
- [24] Y.-L. Park, J. Santos, K. G. Galloway, E. C. Goldfield, R. J. Wood, in *2014 IEEE Int. Conf. on Robotics and Automation (ICRA)*, IEEE, Piscataway, NJ **2014**, pp. 4805–4810.
- [25] Y. Mengüç, Y.-L. Park, H. Pei, D. Vogt, P. M. Aubin, E. Winchell, L. Fluke, L. Stirling, *Int. J. Rob. Res.* **2014**, *33*, 1748.
- [26] P. Ohta, L. Valle, J. King, K. Low, J. Yi, C. G. Atkeson, Y.-L. Park, *Soft Rob.* **2018**, *5*, 204.
- [27] R. Qi, A. Khajepour, W. W. Melek, T. L. Lam, Y. Xu, *IEEE Trans. Rob.* **2017**, *33*, 594.
- [28] E. W. Hawkes, L. H. Blumenschein, *Sci. Rob.* **2017**, *2*, 344.
- [29] S. Sundaram, P. Kellnhofer, Y. Li, J.-Y. Zhu, A. Torralba, W. Matusik, *Nature* **2019**, *569*, 698.
- [30] H. Shi, M. Al-Rubaiai, C. M. Holbrook, J. Miao, T. Pinto, C. Wang, X. Tan, *Adv. Funct. Mater.* **2019**, *29*, 172.
- [31] M. Al-Rubaiai, R. Tsuruta, T. Nam, U. Gandhi, X. Tan, in *Smart Materials Adaptive Structures and Intelligent Systems*, vol. 59131, American Society of Mechanical Engineers, New York **2019**, pp. 112–120.
- [32] H. Zhao, J. Jalving, R. Huang, R. Knepper, A. Ruina, R. Shepherd, *IEEE Rob. Autom. Mag.* **2016**, *23*, 55.
- [33] K. O. Hill, G. Meltz, *J. Lightwave Technol.* **1997**, *15*, 1263.
- [34] H. De la Fuente, J. Raboin, G. Valle, G. Spexarth, in *41st Structures, Structural Dynamics, and Materials Conf. and Exhibit*, Atlanta, GA, USA **2000**, pp. 182–192.
- [35] G. Brown, R. Haggard, B. Norton, in *16th AIAA Aerodynamic Decelerator Systems Technology Conf. and Seminar*, Boston, MA, USA **2001**, pp. 206–214.
- [36] Y. Song, U. Gandhi, A. Aris, in *AIAA Scitech Forum*, **2021**, pp. 430–437.
- [37] H. Gabriel, *Appl. Ergon.* **2020**, *84*, 103006.
- [38] R. E. Freeland, G. D. Bilyeu, G. R. Veal, M. D. Steiner, D. E. Carson, *Acta Astronaut.* **1997**, *41*, 267.
- [39] M. Kalantari, J. Dargahi, J. Kövecses, M. G. Mardasi, S. Nouri, *IEEE/ASME Trans. Mechatron.* **2011**, *17*, 572.
- [40] R. Berman, D. K. C. Macdonald, *Proc. R. Soc. London Series A* **1952**, *211*, 122.
- [41] R. Hudec, S. Matúška, P. Kamencay, M. Benco, *Sensors* **2021**, *21*, 206.
- [42] X.-W. Zhang, Y. Pan, Q. Zheng, X.-S. Yi, *J. Polym. Sci. Part B: Polym. Phys.* **2000**, *38*, 2739.
- [43] A. Dzedzickis, E. Sutinyus, V. Bucinskas, U. Samukaite-Bubniene, B. Jakstys, A. Ramanavicius, I. Morkvenaite-Vilkonciene, *Polymers* **2020**, *12*, 2905.
- [44] L. Shen. PhD thesis, University of Akron, **2015**.
- [45] K. Ehrmann, *Int. Young Physicists Tournament (IYPT)* **2011**, *33* 122.
- [46] S. Sridar, S. Poddar, Y. Tong, P. Polygerinos, W. Zhang, *IEEE Rob. Autom. Lett.* **2020**, *5*, 4062.
- [47] F. London, *Rev. Mod. Phys.* **1945**, *17*, 310.
- [48] G. Gräff, H. Kalinowsky, J. Traut, *Z. Phys. A Atoms Nucl.* **1980**, *297*, 35.